COHERENT VORTICAL AND STRAINING STRUCTURES IN THE FINITE WALL-MOUNTED SQUARE CYLINDER WAKE

J. A. Bourgeois, P. Sattari, R. J. Martinuzzi
Deptartment of Mechanical and Manufacturing Engineering
University of Calgary
2500 University Drive NW, Calgary, Alberta, T2N 1N4, Canada
jabourge@ucalgary.ca, psattari@ucalgary.ca, rmartinu@ucalgary.ca

ABSTRACT

Topological aspects of the turbulent wake of a finite, surface-mounted, square-cross-section cylinder of $h/d = 4$ are addressed by decomposing the velocity field into a quasi-periodic coherent part and deviations therefrom as unresolved incoherent fluctuations. The three-dimensional large scale structure is educed through a reconstruction of phase-averaged PIV *x-y* and *x-z* measurement planes using the simultaneously sampled surface pressure difference on either side of the obstacle as a phase reference. A topological model for the vortex structure is educed and an explanation for mean streamwise wake vorticity is given in terms of the connections between initially vertical structures shed alternately from either side of the obstacle, rather than 'tip' vortex structures generated at the obstacle free-end as proposed in other studies. The coherent structure educed accounts for a significant portion of the fluctuating energy in the wake. The turbulent field is analyzed by finding Lagrangian straining structures that form by induction of the vorticity field, and these structures are related to the energy transfer from the base phase-averaged flow.

INTRODUCTION

Turbulent finite bluff body wakes contain a very significant amount of organization at the energetic large scales in the form of quasi-periodic vortex shedding. The large scale vortices are important as they govern the organized mixing of passive tracers in the wake by induction processes. In the case of pollutant dispersion in the wakes of buildings and stacks, this is particularly important as the streamwise vorticity field towards the free-end of these structures tends to induce flow down toward the ground. The prediction and control of wake transport processes requires an understanding of the coherent vortex structures due to the fundamental role they play in mixing and dispersion.

In the wake of finite surface-mounted cylinders the existence of mean streamwise vorticity has been observed for some time (Etzold and Fiedler, 1976; Kawamura et al., 1984; Mason and Morton, 1987). Recent studies have shown dramatic changes occuring in the mean streamwise vorticity distribution as the aspect ratio, h/d, is varied (h is the height and d the width of the cylinder). Sumner et al. (2004) and Wang and Zhou (2009), respectively, showed that a change occurs between $h/d = 3$ and 5 for circular- and square-cross-section cylinders. Above this critical value, a quadrupole mean streamwise vorticity distribution occurs well downstream of the recirculation zone (two sets of counter-rotating vortices at the top and bottom of the wake) while a dipole distribution occurs for aspect ratios below the critical value. Basic questions about whether the mean streamwise vorticity is due to steady (independently existing) streamwise structures originating at the free-end of the obstacle as described in Etzold and Fiedler (1976) or are a result of the unsteady large scale vortex structures have been expressed (Sumner et al., 2004) but still not resolved. In a forthcoming article, Bourgeois et al. (2011) have shown that the resulting mean vorticity field has little to do with streamwise structures generated at the leading corners of the obstacle, but rather is an artefact of the averaging of the convecting and deforming coherent structures shed from the obstacle. Differences in the topology of shed structures has an impact on the turbulence field, and it is shown that the interpretation of the streamwise vorticity being due to the three-dimensional large scale structures better explains the turbulence fluctuating field observed. Topological arguments about the source of turbulence production being convective saddle-points (Cantwell and Coles, 1983; Hussain, 1986) are generalized to three-dimensions using Lagrangian coherent structures concepts.

A detailed experimental study of a finite square-cross-section cylinder was conducted in order to directly educe the three-dimensional large scale vortex structure and study the interaction of the large scale structure on the turbulent field. The large scale coherent field is calculated by phase averaging (Hussain, 1983) and straining structures of the phase averaged field are found using ridges of the finite time Lyapunov exponent field (Haller, 2001; Shadden et al., 2005).

EXPERIMENTAL SETUP

Measurements were conducted in an open-test-section suction wind tunnel, shown schematically in Fig. 1. A base turbulent boundary layer is generated using a sharp leading edge flat plate. In the absence of the obstacle, the bound-

ary layer thickness at the obstacle mounting location is δ/h = 0.18. Free-stream test conditions were U_∞ = 15 m/s, corresponding to a Reynolds number $Re = U_\infty d/\nu$ = 12,000, and 0.8% turbulence intensity. A Strouhal number of $St = fd/U_\infty = 0.100 \pm 0.003$ (f the vortex shedding frequency) was found for the h/d = 4 square-cross-section cylinder.

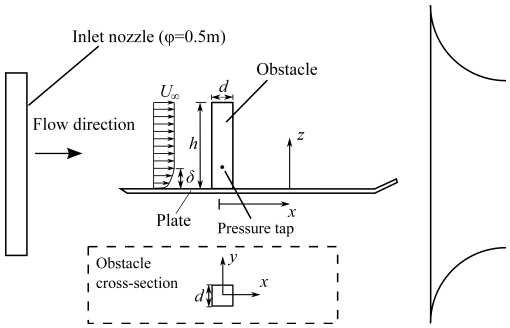

Figure 1. Schematic of experimental setup of the working section of the wind tunnel (not to scale) with the nomenclature and coordinate system definition shown.

A grid of several horizontal (x-y) and vertical (x-z) planes with a spacing of $d/4$ or less were measured using a LaVision FlowMaster high-frame-rate particle image velocimetry (PIV) system. These planar measurements are used to reconstruct the phase averaged three dimensional flow. A pulse separation of 50μs was used and frame rates of 500 to 1000Hz captured 4 to 8 data points per shedding cycle.

The experimental study of unsteady complex turbulent flows suffers from a key difficulty: the flow field is inherently three-dimensional but the large number of data points needed to resolve the coherent structures of interest is impractical to measure simultaneously. We first show that the most energetic structures are quasi-periodic and then we take advantage of the periodicity in order to reconstruct in three-dimensions a synchronized phase averaged field. In order to have a consistent phase reference to synchronize all measurements, the fluctuating surface pressure at $z/h = 0.25$ on either side of the cylinder is measured simultaneously and subsequently analyzed to find the instantaneous phase of the shedding cycle for each velocity field. The sampling rate for the reference surface pressure is 10.24 kHz and is sychronized with the PIV measurements using a TTL trigger. The shedding period is discretized into twenty equal phase steps, $\phi_n = n\Delta\phi$, ($\Delta\phi = \pi/10$) where $\phi(t) \in [0, 2\pi)$. A double decomposition ensemble average (Hussain, 1983) conditional upon the phase falling within the interval $\phi_n - \Delta\phi/2 \leq \phi_n < \phi_n + \Delta\phi/2$ is undertaken for each phase step.

PHASE AVERAGING FOR COHERENT STRUCTURE EDUCTION

The primary energetic eddies in the finite body wake are large scale and are shed from the body quasi-periodically. This can be verified, in a spatially integrated sense, by computing the proper orthogonal decomposition (POD) of the unsteady field (Lumley, 1967; Holmes et al., 1996) for a given horizontal PIV plane (note that the v' fluctuations are largest in the wake, and so a horizontal plane is an appropriate choice to study the most energetic structures),

$$\mathbf{u}(\mathbf{x},t) \simeq \overline{\mathbf{u}}(\mathbf{x}) + \sum_{k=1}^{N} a^{(k)}(t)\mathbf{u}^{(k)}(\mathbf{x}) \tag{1}$$

where $\overline{\mathbf{u}}(\mathbf{x})$ is the time averaged flow, $a^{(k)}(t)$ are the modal Fourier coefficients, and $\mathbf{u}^{(k)}(\mathbf{x})$ are the spatial eigenmodes of the fluctuations. Due to the optimality of the decomposition in terms of energy, the best two-mode ($N = 2$) approximation of the unsteady field is given by the first two POD modes. For these modes, the coefficients $a^{(1)}(t)$ and $a^{(2)}(t)$ are nearly periodic and form a sine-cosine pair (Fig. 2). The fact that the most energetic structures contributing to the fluctuations are quasi-periodic allows us to synchronize phase averaged planar fields using a consistent reference phase of the shedding event associated with each measured PIV vector field.

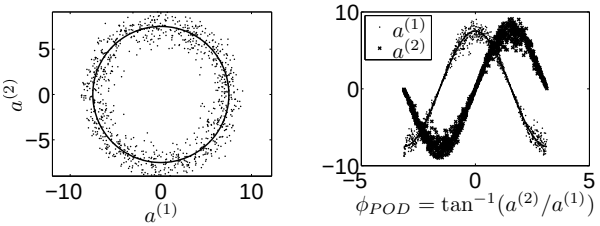

Figure 2. Coefficients $a^{(1)}(t)$ and $a^{(2)}(t)$ of the POD decomposition of 1000 PIV measurements in the plane $z/h = 0.3125$. The circle defined by the mean amplitude is shown.

The phase of the fluctuating pressure difference on either side of the obstacle at $z/h = 0.25$ is used as a consistent reference phase. Figure 3 shows the fluctuating pressure difference and the phase that was determined by interpolation over peak-to-peak intervals in the signal. As the frequency of interest is the vortex shedding frequency, the high-frequency content of the signal was removed using a truncated Fourier series reconstruction with 2000 modes from a 100,000 point sample. This resolves up to approximately 200 Hz, nearly twice the shedding frequency of 120Hz.

The analysis procedes by decomposing the velocity field into a base flow which is periodic and any deviations therefrom are considered incoherent turbulent fluctuations.

$$\mathbf{u}(\mathbf{x},t) = \langle \mathbf{u} \rangle (\mathbf{x}, \phi(t)) + \mathbf{u}''(\mathbf{x},t) \tag{2}$$

Unlike the Reynolds decomposition where $\overline{\mathbf{u}}(\mathbf{x})$ is taken as the base flow and $\mathbf{u}'(\mathbf{x},t)$ the fluctuations, now the base flow which provides energy to the turbulent fluctuations, $\mathbf{u}''(\mathbf{x},t)$, is the phase averaged field, $\langle \mathbf{u} \rangle (\mathbf{x}, \phi(t))$, and the energy exchange occurs through the turbulence production term, $P_{k''} = \left\langle u_i'' u_j'' \right\rangle \partial \langle u_i \rangle / \partial x_j$. We also define the Reynolds decomposition of the phase averaged field, $\langle \mathbf{u} \rangle (\mathbf{x}, \phi(t)) = \overline{\mathbf{u}}(\mathbf{x}) +$

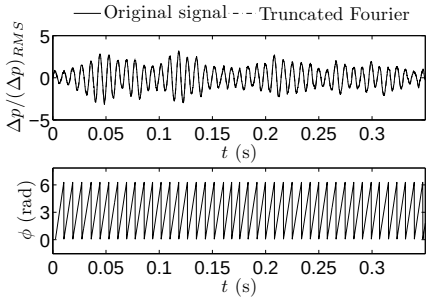

Figure 3. Determination of phase from the pressure difference ay $z/h = 0.25$ on either side face of the obstacle.

$\tilde{\mathbf{u}}(\mathbf{x},\phi(t))$ where the total Reynolds averaged fluctuations are therefore a combination of the coherent and incoherent contributions, $\mathbf{u}'(\mathbf{x},t) = \tilde{\mathbf{u}}(\mathbf{x},\phi(t)) + \mathbf{u}''(\mathbf{x},t)$.

STRAINING COHERENT STRUCTURES

Turbulence production mechanisms transferring energy between the coherent and incoherent fields are commonly attributed to vortex stretching. As such, the process is inherently related to relative Lagrangian motion between fluid particles convected by the flow, in this instance the phase averaged velocity field, $\langle\mathbf{u}\rangle$. Lagrangian coherent structures concepts, therefore, can be used to help distinguish regions of importance for the turbulence transport and production processes in the unsteady phase averaged field. In two-dimensional flows, high production has been ascribed to stretching of incoherent vortices in the neighbourhood of convective frame saddle-points tangent to the unstable manifold by Cantwell and Coles (1983) for the circular cylinder wake and by Hussain (1986) for the mixing layer. Convective frame saddle-point arguments neglect unsteadiness, instead assuming a frozen translating velocity field. Lagrangian coherent straining structures are able to properly account for the true unsteady relative motion of particles being advected, providing a more accurate means of determining high-production regions.

The phase averaged vortex structure induces attracting and repelling manifolds. In time-invariant fields, these manifolds would correspond to unstable and stable manifolds, respectively. Stretching of vortices in the incoherent fluctuating field by the manifolds leads to amplification of vorticity, and transfer of energy from large to small scales. Ridges of the finite time Lyapunov exponent (FTLE) field, $\sigma_{t_0}^{T}$ — which measures how much particles separate from one another over a given finite time interval — provide a means to determine these manifolds (Haller, 2001; Shadden et al., 2005), where

$$\sigma_{t_0}^{T}(\mathbf{x}) = \frac{1}{|T|}\ln\sqrt{\lambda_{max}(\Delta)} \tag{3}$$

$\lambda_{max}(\Delta)$ is the maximum eigenvalue of the Cauchy-Green deformation tensor, Δ, computed for the time t_0 over an integration time T for the flow map $\phi_{t_0}^{t_0+T}$. The Cauchy-Green deformation tensor is defined as

$$\Delta = \frac{d\phi_{t_0}^{t_0+T}(x)}{dx}^{*}\frac{d\phi_{t_0}^{t_0+T}(x)}{dx} \tag{4}$$

In order to evaluate the FTLE numerically, a grid of particles is advected using a fourth-order Runge-Kutta method using spatial trilinear interpolation of the flow data. Gradients of the flow map are obtained by second-order finite differencing for the evaluation of the Cauchy-Green deformation tensor.

Forward time integration of particles yields repelling manifolds in the FTLE field while backward time integration yields attracting manifolds (Fig. 4). Both types of manifolds determine the general tendencies of the phase averaged flow to stretch incoherent vorticity. Fluctuating vortex lines transverse to repelling surfaces are stretched normal to the surface, while fluctuating vortex lines parallel to attracting surfaces get stretched tangent to the surface. In either case vorticity is amplified and fluctuating energy transferred to smaller scales. The attracting and repelling manifolds also provide trapping regions for turbulent fluid because there is negligible mass flux across ridges of the FTLE field (Shadden et al., 2005). Although turbulent transport by the fluctuations still provides a diffusion-type mechanism for turbulence quantities across the Lagrangian manifolds, they do provide a convective transport barrier, yielding important insights into the mixing induced by the large scale structures.

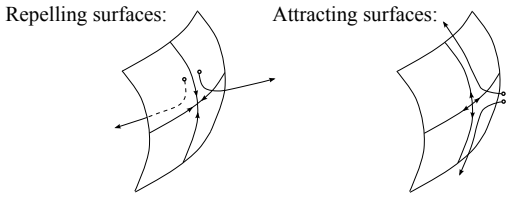

Figure 4. Attracting and repelling surfaces and their stretching effect on material lines connecting adjacent fluid particles.

RESULTS

The phase averaged velocity and Reynolds stress fields were reconstructed in 3D by trilinear interpolation of the PIV data. The results show that initially, the side-face separated shear layers roll-up along the height of the obstacle (see the vorticity plots in Fig. 5 and the identified vortex structures in Fig. 6), forming tubular vortices that subsequently deform three-dimensionally as they convect downstream.

The phase averaged vortex structure can be identified using standard Galilean invariant methods since all components of the deformation tensor, $\partial\langle u_i\rangle/\partial x_j$, are known from the three-dimensional reconstruction. Figure 6 shows the vortex structure identified by the λ_2-criterion (Jeong and Hussain, 1995) for the first phase instant, $\phi_1 = \pi/10$. After formation, the top portion of the rolled-up vortex deforms and is bent backwards by the induction of the free-end separated vorticity. The shed structure once fully formed shows a near vertical orientation in the principal core (terminology as per the sketches in Fig. 6) near the ground plate, and a branching outwards horizontally where the vortex structures interact with

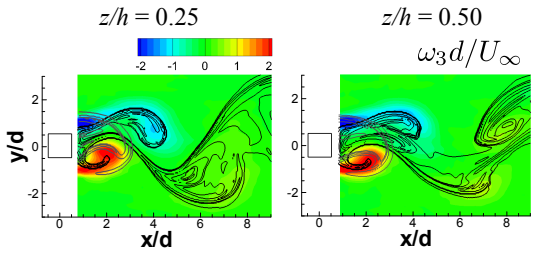

Figure 5. Positive time (grey lines) and negative time FTLE contours (black lines) shown with $\omega_3 d/U_\infty$ (colour contours) at ϕ_1 where $\omega_i = \varepsilon_{ijk}\partial\langle u_k\rangle/\partial x_j$.

the boundary layer vorticity. Downstream of the formation region, highly inclined (nearly streamwise) connector strands cross from the top of the principal core of one structure to the bottom of the subsequently shed principal core on the opposite side of the wake, resulting in a highly three-dimensional vorticity and induced strain field.

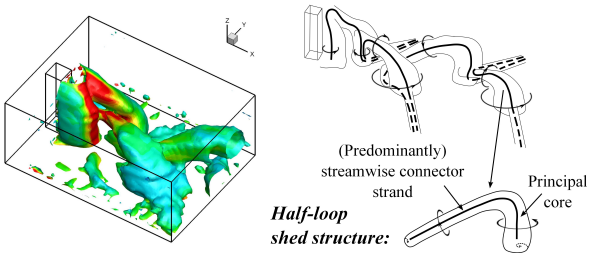

Figure 6. Isosurface of the phase averaged $\lambda_2 = -0.02$ coloured by the vorticity magnitude, $\|\omega\|$ at ϕ_1.

The time averaged wake is found to be typical of lower aspect ratio wakes in terms of streamwise vortex structure (Sumner et al., 2004; Wang and Zhou, 2009). The λ_2-criterion can be again applied to identify the mean vortex structure as in Fig. 7 (with an isosurface $\lambda_2 = -0.02$), showing an arch vortex with counter-rotating legs recirculating flow in the base region of the obstacle, and a nearly horizontal hairpin structure whose streamwise extensions induce downwash along y/d=0 at the top of the wake. Although unclear from previous studies, the phase averaged field demonstrates that mean streamwise vortex structures arise due to the time averaging of the streamwise connector strands of the half-loop shed vortices. Only one sense of streamwise vorticity is felt at the top of the wake on either side of $y/d = 0$ resulting upon averaging in a counter-rotating vortex pair due to the connection of the top of the principal core across the wake to the bottom of the opposing successively shed structure.

The phase averaged field is better able to localize and explain the transport and energy transfer occuring between the deterministic large scale coherent vortices and the smaller scale randomly occuring vortices. The decomposition of the velocity field results in a split of the total Reynolds stress and turbulent kinetic energy fields into coherent and incoherent components. That is, for the phase averaged field, $\left\langle u_i' u_j' \right\rangle = \tilde{u}_i\tilde{u}_j + \left\langle u_i'' u_j'' \right\rangle$ and for the time averaged field,

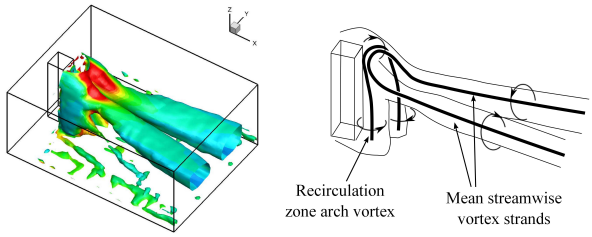

Figure 7. Isosurface of the time averaged field $\lambda_2 = -0.02$ coloured by the vorticity magnitude, $\|\Omega\|$.

$\overline{u_i' u_j'} = \overline{\tilde{u}_i\tilde{u}_j} + \overline{u_i'' u_j''}$ where the first and second terms are the coherent and incoherent contributions, respectively. The coherent fluctuating field is resolved and can be explained in terms of induction by the vorticity field and the resulting mean flow. The incoherent field, however, is unresolved, but the energy transfer from the coherent to the incoherent field occurs through the production term, $P_{k''}$, which is a non-linear interaction of the two fields. As Cantwell and Coles (1983) and Hussain (1986) have done for 2D flows, we seek the correspondence between the incoherent turbulence production and the topology of the strain field induced by the coherent vortices to better understand energy transfer in the 3D wake.

To do so, the Lagrangian straining structures in the wake are sought by calculating the FTLE field with time parameters (non-dimensionalized by d/U_∞) $t_0 = \phi_1/2\pi St$ and $T = \pm 10$. The only repelling surfaces found for the $\langle \mathbf{u} \rangle$ field are in the formation region (Fig. 8, left). Attracting surfaces are much more abundant in the wake (Fig. 8, right)

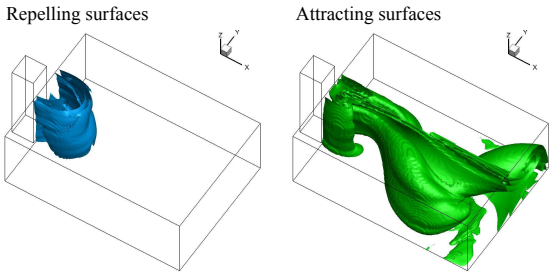

Figure 8. Positive time (left, $\sigma^T_{t_0} = 0.150$) and negative time (right, $\sigma^T_{t_0} = 0.185$) FTLE iso-surfaces.

Iso-surfaces of the highest values of production do in fact correspond to the attracting surfaces, as shown in Fig. 9. The planes shown are $z/h = 0.25$ which cuts through the vertical principal core and the plane $z/h = 0.50$ which is the underside of a streamwise connector strand crossing $y = 0$ to the principal core at $x/d = 7$ and $y/d = -2$. The topology of the stretching surface induced by the vortices leads to increased straining due to the presence of the streamwise connector strands in the finite three-dimensional wake and leads to increased production at regions slightly below the streamwise portion of the strand at the top of the wake (Fig. 9, right). Note that in the calculation, all terms are accounted for in $P_{k''}$ except $\langle v''w'' \rangle \left(\frac{\partial \langle v \rangle}{\partial z} + \frac{\partial \langle w \rangle}{\partial y} \right)$ since $\langle v''w'' \rangle$ was

not measured. The Cauchy-Schwarz inequality, $|\langle v''w''\rangle| \leq \left(\langle v''^2\rangle \langle w''^2\rangle\right)^{1/2}$, bounds this contribution, and it is estimated that the resulting production will not differ by more than 5% by including this term.

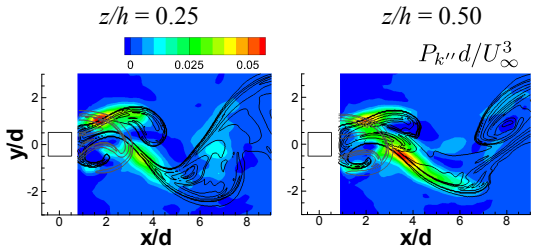

Figure 9. Positive time (grey lines) and negative time FTLE contours (black lines) shown with the production, $P_{k''}$ (colour contours) at ϕ_1.

Before describing the coherent/incoherent split of the Reynolds stresses, the resolved coherent fluctuations—$\tilde{u}$, $\tilde{v}$, and $\tilde{w}$ are discussed (Fig. 10). In a uniform time-averaged velocity field, fluctuations are simply related to the induction of instantaneously passing vortices. In a non-uniform flow such as the wake, the induction of vortex structures is partly accounted for by the mean field, so the fluctuating field around a vortex structure is not obvious from the vorticity field alone. For the coherent vortex structures educed, large $\tilde{u}$ fluctuations occur on the outer edges of the wake. The mean velocity at these locations is not as high as the induced velocity by the passing vortices, and so positive extrema of $\tilde{u}$ arise in the presence of a passing vortex while negative extrema arise in the absence of a vortex. The amplitude of the extrema of $\tilde{u}$ decrease with streamwise location as the vortex strength decays. In the centre of the wake, fluctuation amplitudes of $\tilde{u}$ are very small despite passing structures of opposite sign. Here, the backflow induced by Biot-Savart induction is approximately constant no matter the phase of the cycle, and thus the induction becomes part of the mean. The $\tilde{v}$ fluctuation, on the other hand, is high on the up- and downstream sides of each coherent vortex, and is highest along $y = 0$ directly in between the vortices of either sign of ω_3 where the sign of the induced $\tilde{v}$ changes with the passage of each differently signed vortex. The $\tilde{w}$ fluctuation behaves as an almost purely inductive effect since outside the formation region, the mean vertical velocity is quite small. The induced velocity results in maxima and minima of $\tilde{w}$ on the exterior and interior sides, respectively, of the connector strands.

The coherent, $\tilde{u}_i\tilde{u}_j$, and incoherent, $\left\langle u_i''u_j''\right\rangle$, components of three of the phase averaged total Reynolds stress, are shown in Figs. 11 and 12 (other Reynolds stresses are not shown due to space limitations). There is a strong dominance of the resolved $\tilde{v}^2$ (peaks of $\tilde{v}^2$ are typically about 5 to 20 times higher than $\langle v''^2\rangle$) and $\tilde{u}\tilde{v}$ (peaks are about 5 times larger) over the respective incoherent components. To a lesser extent, the same is true of $\tilde{u}\tilde{w}$ as well (peaks are about 3 times larger). As with $\tilde{v}$, the $\tilde{v}^2$ stress is high at locations between two opposite signed vortices. The correlation between the $\tilde{u}$ and $\tilde{v}$ components gives rise to patches of one sign of $\tilde{u}\tilde{v}$ only on either side

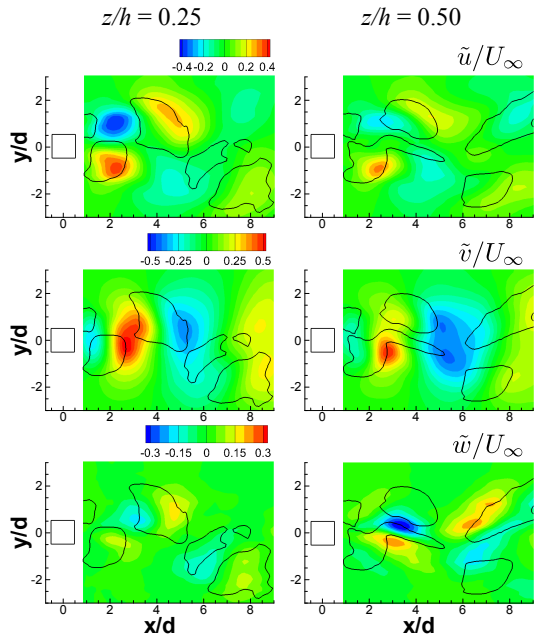

Figure 10. $\lambda_2 = -0.05$ (black lines) shown with $\tilde{u}_i/U_\infty$ (colour contours) at ϕ_1.

of the wake that corresponds to the same sign as the vorticity in the separated shear layer. There is not a particularly good correlation between $\tilde{u}$ and $\tilde{w}$ ($\tilde{u}\tilde{w}$ is about an order of magnitude lower than the other components), and thus the $\tilde{u}\tilde{w}$ is of less importance than the other Reynolds stresses.

Since the total separated vorticity is not contained within the large-scale structures, subsequent instability and roll-up of smaller-scale structures occurs, which is enhanced by the straining field of the phase-averaged flow. This gives rise to additional small scale structures of the same rotational sense as the large on either side of the wake, as can be seen in the contours of $\langle u''v''\rangle$ (Fig. 12). One can expect the fluctuating fields around the small scale structures to be similar to those around the large, but upon averaging, the distributions are smeared out since the time scales of the primary vortex shedding instability and those of the small scale instabilities are uncorrelated. The incoherent stresses in Fig. 12 are consistent with only a small flux (associated with diffusive turbulent transport) across ridges of the FTLE field, and thus the majority of the turbulent kinetic energy gets trapped by the manifolds. Turbulent energy is gathered by the large scale structure into vortex cores, as is apparent for the localized high levels of $\tilde{v}^2$ in the trapping regions of the vortices (Fig. 12). As mentioned previously, in the FTLE ridge just below the regions of highest streamwise vorticity, very high coherent strain rates are found, corresponding to peaks of production of incoherent turbulence (Fig. 9). This production term is primarily due to the $\langle u''v''\rangle$ term which is high along the attractive manifold ridges of the FTLE.

CONCLUDING REMARKS

This study resolves the phase-averaged topology of the shed vortices in the wake of a finite wall-mounted body. The phase-averaged decomposition splits Reynolds stresses and

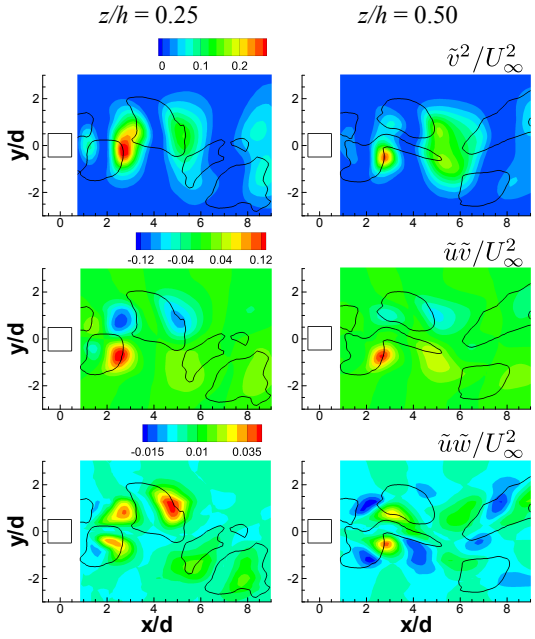

Figure 11. $\lambda_2 = -0.05$ (black lines) shown with $\tilde{u}_i\tilde{u}_j/U_\infty^2$ (colour contours) at ϕ_1.

turbulent kinetic energy into a coherent component arising from induced velocities by the large-scale vortices and an incoherent component that remains an integrated effect of uncorrelated small-scale vortices. This description allows the incoherent turbulent field to be described in terms of the phase-averaged base flow environment in which it is found. The shed structure consists of alternating and deformed half-loop streamwise-interconnected structures which branch outward at the surface of the plate, interacting with the outer boundary layer vorticity. Topological concepts of induced straining in the vicinity of the unstable manifold of convective saddle-points between vortices have been generalized to three-dimensions using Lagrangian coherent structures concepts. In a similar manner to the unstable manifolds of convective saddles in 2D wakes, the attractive manifolds of the finite wake enveloping the coherent structures are found to be responsible for the majority of incoherent turbulence production and thereby have a large impact on the turbulent fluctuations and Reynolds stresses in their neighbourhood.

REFERENCES

Bourgeois, J. A., Sattari, P., and Martinuzzi, R. J., 2011, "Alternating half-loop shedding in the turbulent wake of a finite surface-mounted square cylinder with a thin boundary layer", Submitted Feb. 2011 to Phys. Fluids (under review).

Cantwell, B. and Coles, D., 1983, "An experimental study of entrainment and transport in the turbulent near wake of a circular cylinder", J. Fluid Mech., Vol. 136, pp. 321–374.

Etzold, F. and Fiedler, H., 1976, "Near-wake structure of a cantilevered cylinder in a cross-flow", Z. Flugwiss., Vol. 24(2), pp. 77–82.

Haller, G., 2001, "Distinguished material surfaces and coherent structures in three-dimensional fluid flows", Physica D, Vol. 149, pp. 248–277.

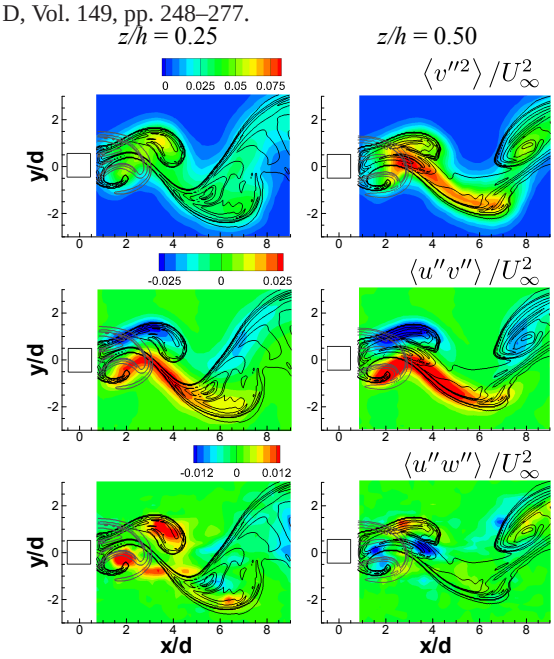

Figure 12. Positive time (grey lines) and negative time FTLE contours (black lines) shown with $\left\langle u_i'' u_j'' \right\rangle / U_\infty^2$ (colour contours) at ϕ_1.

Holmes, P., Lumley, J. L., and Berkooz, G., 1996, Turbulence, Coherent Structures, Dynamical Systems and Symmetry, Cambridge University Press.

Hussain, A. K. M. F., 1983, "Coherent structures—reality and myth", Phys. Fluids, Vol. 26(10), pp. 2816–2850.

Hussain, A. K. M. F., 1986, "Coherent structures and turbulence", J. Fluid Mech., Vol. 173, pp. 303–356.

Jeong, J. and Hussain, F., 1995, "On the identification of a vortex", J. Fluid Mech., Vol. 285, pp. 69–94.

Kawamura, T., Hiwada, M., Hibino, T., Mabuchi, I., and Kumada, M., 1984, "Flow around a finite circular cylinder on a flat plate. cylinder height greater than turbulent boundary layer thickness", Bulletin of the JSME, Vol. 27(232), pp. 2142–2151.

Lumley, J. L., 1967, "The structure of inhomogeneous turbulence", in A. M. Yaglom and V. I. Tatarski, eds., Atmospheric Turbulence and Radio Wave Propagation, Nauka, Moscow, pp. 166–178.

Mason, P. J. and Morton, B. R., 1987, "Trailing vortices in the wakes of surface-mounted obstacles", J. Fluid Mech., Vol. 175, pp. 247–293.

Shadden, S. C., Lekien, F., and Marsden, J. M., 2005, "Definition and properties of Lagrangian coherent structures from finite-time Lyapunov exponents in two-dimensional aperiodic flows", Physica D, Vol. 212, pp. 271–304.

Sumner, D., Heseltine, J. L., and Dansereau, O. J. P., 2004, "Wake structure of a finite circular cylinder of small aspect ratio", Exp. Fluids, Vol. 37, pp. 720–730.

Wang, H. F. and Zhou, Y., 2009, "The finite-length square cylinder near-wake", J. Fluid Mech., Vol. 638, pp. 453–490.